



Research on abrasive pool machining method based on gas–solid two-phase flow

Wei Yuan^{1,2} · Wenhua Wang¹ · Qianjian Guo¹ · Xuehu Lv¹ · Xingcan Wang^{1,3} · Baotao Chi¹

Received: 28 June 2022 / Accepted: 7 November 2022 / Published online: 18 November 2022
© The Author(s), under exclusive licence to Springer-Verlag London Ltd., part of Springer Nature 2022

Abstract

For complex curved difficult-to-machine parts, a new method based on pneumatic suspension abrasive pool bright finishing processing is proposed, using the mixing of pneumatic suspension abrasive, the workpiece surface, and fluidized abrasive to produce relative motion velocity, so that the solid particles and workpiece surface microscopic two-body abrasive wear to achieve the effect of precision machining. The experimental test material is the widely used Q235 steel plate. The experimental parameters include workpiece shape (round tube, square tube, cylindrical), abrasive particle size (24, 80, 120 mesh count), gas–solid two-phase flow pattern (dispersion fluidization state, turbulent fluidization state, spurting fluidization state), abrasive particle shape (sphere, irregular), and spindle speed (600, 900, 1200 rpm). An orthogonal test was designed according to the experimental parameters, and the degree of influence of each parameter on the processing of the abrasive cell was evaluated by the roughness of the workpiece surface together with the scanning electron microscope (SEM) micrograph of the workpiece surface, and the optimal combination of parameters was judged using the extreme difference method as well as the factor trend diagram. The results show that under the present experimental conditions, the workpiece surface roughness (Ra) can reach a minimum value of 0.4 μm . The feasibility of gas–solid two-phase flow processing is demonstrated from an experimental point of view, and the advantages of abrasive cell processing are explored.

Keywords Abrasive pool · Gas–solid two-phase flow · Finish machining · Surface quality

1 Introduction

The manufacturing industry is the top priority in the development of national machinery industry, among which polishing process, as the main processing technology to improve the surface quality of products, is an indispensable process for every spare part to be processed. The surface quality of metal workpiece has an important influence on its performance and life. With the continuous development of cutting-edge manufacturing technology, the surface shape of ultra-precision parts has gradually extended from a simple plane to a more complex surface and has been widely

used in aerospace, biomedical, marine exploration, and other fields, such as aero-engine blade and human bone implant. Traditional processing methods have been difficult to meet the industry demand and production requirements.

In order to reduce surface roughness, surface damage is removed, so that parts can achieve ultra-high machining accuracy and surface quality. At present, the main finishing methods in the world are mechanical, magnetorheological, electrorheological, magnetic levitation, and chemical polishing. Alam and Jha [1], Grover and Singh [2], Mandal et al. [3], and Lin et al. [4] respectively studied the magnetorheological polishing modeling, chemical mechanical polishing process, equipment development, and other issues. However, the above processing methods have obvious defects, such as low mechanical polishing processing quality and poor processing efficiency. The electromagnetic processing is expensive and the cost is high, and the processing parts are also limited. Chemical polishing easily produces chemical waste and pollutes the environment. The traditional polishing process is greatly affected by the workpiece shape, and it is difficult to process complex and irregular surfaces.

✉ Qianjian Guo
guojq_xs@163.com

¹ School of Mechanical Engineering, Shandong University of Technology, Zibo 255049, China

² Tianrun Industrial Technology Co., LTD, Weihai 264200, China

³ GoerTek Co., LTD, Weifang 261000, China

Therefore, based on the principle of “fluidized bed,” this paper proposes a pneumatic suspended abrasive pool finishing method, which has the advantages of high efficiency, high precision, low cost, no pollution, and a wide range of applications.

Guo et al. [5] determined different cutting characteristics between abrasive particles and workpieces at different positions based on magnetic flux changes, while Wang et al. [6] found that different air pressure directions could form different impact cutting effects, and also analyzed different impact grinding behaviors of gas–solid two-phase jet on the surface, including different abrasive particle residence time and density distribution [7], which have different effects on the surface roughness. By studying the impact grinding behavior of abrasive particles [8–10], researchers also found that the surface roughness is positively correlated with the impact angle, the impact trajectory of abrasive particles can be changed by using spiral constraint abrasive flow, and the surface quality of workpiece can be effectively improved.

In addition, the researchers also found that the surface roughness and grain quality score, grinding grain and workpiece materials, grinding grain size, edge sharpness, cutting force, and surface shear strength are closely related to the time and the whole processing parameters such as grits [11, 12], but when the abrasive grain reaches a certain size, its impact on the surface can change the surface microstructure composition [13]. In this way, the surface density, microhardness, wear resistance, and fatigue resistance are improved [14–20]. Shot peening achieves such effects [21].

However, if the abrasive particle size is further increased, it will hurt the surface roughness. To solve this problem, Maleki et al., Pritima et al., and Mohamed et al. [22–24] in the field of shot peening provided a good solution. Finally, on the condition of obtaining excellent surface mechanical properties, the ideal surface roughness is obtained.

To sum up, through the abrasive particle flow, particle size, particle morphology, particle velocity, inlet flow rate,

pressure of abrasive flow machining parameters, such as comprehensive control, metal surfaces can be finished, to obtain ideal surface roughness, based on realization of gas–solid two-phase particle flow on the surface of metal microstructure control.

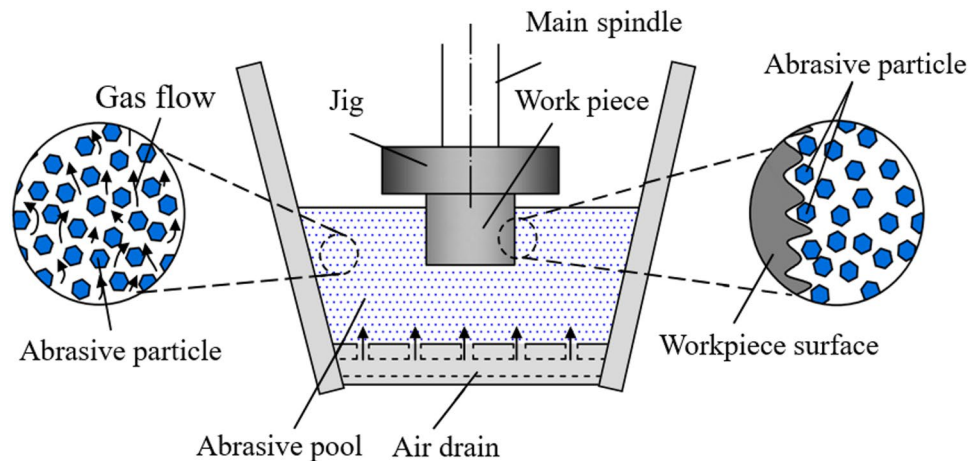
2 Basic principle of abrasive pool machining

2.1 Processing schematic diagram

According to the basic principle of fluidized bed, a finishing method based on “abrasive flow” was adopted in this paper. As shown in Fig. 1, a large number of solid abrasive particles were mixed with high-pressure gas to form a fluidization abrasive flow of solid abrasive particles, and the workpiece was placed in the confined place of abrasive flow. Friction and micro-cutting would occur on the workpiece surface caused by the flowing abrasive particles, so as to realize the finishing processing of the workpiece with well surface quality.

Pneumatic suspension abrasive pool finishing is a new precision machining method. In such an approach, the mechanical energy of high-speed abrasive will be converted into the elastic deformation energy, plastic deformation energy, and surface energy of the processed material to effectively improve the machining efficiency. Based on the principle of heavy floating coupling, the mixing mode of pneumatic suspended abrasive is adopted to produce the relative velocity between the workpiece surface and the fluidized abrasive, so that the micro-two-body abrasive wear occurs between the solid particles and the workpiece surface. By using such kind of flexible micro-grinding method, the workpiece surface can achieve ultra-precision finishing effect [25–27].

Fig. 1 Processing schematic diagram



2.2 Mechanism of gas–solid two-phase flow machining

Under the action of high-pressure gas, the solid particles show a flow-solid contact state, when the gas–solid two-phase flow is in contact with the surface of the workpiece, the solid particles will have a mechanical polishing effect on that surface. The mixing of gas and abrasive has an important influence on the gas–solid reaction, and its diffusion law has become the main influencing factor of many reaction processes. In order to reveal the microscopic and transient structural parameters and their variation laws, the Reynolds number of abrasive particles will be determined. Abrasive particles are assumed to be spherical, and the radius of envelope sphere is represented by the symbol r_s , as shown in Fig. 2; thus, the slip velocity is calculated as follows:

$$\vec{e} = \vec{Q} / |\vec{Q}| \tag{1}$$

$$\vec{Q} = \iint_{\Omega_{r_s}} [(u - u_p) \cdot n] nd\sigma \tag{2}$$

where e represents the direction of fluid motion relative to the abrasive particles outside the envelope sphere; Q represents the net relative flux of fluid through the envelope sphere; Ω_{r_s} is the envelope sphere boundary; u is the fluid velocity vector; u_p is the particle center-of-mass linear

velocity; n is the normal unit vector; σ is the envelope sphere great circle circumference.

Once the value of e is determined, the velocity of fluid motion relative to the abrasive grain can be calculated by projecting the velocity difference between the fluid and the abrasive grain in that direction. Finally, the slip velocity can be obtained by referring to Kidanemariam’s method.

$$u_{rel} = (u - u_p) \cdot e \tag{3}$$

$$u_{slip} = \frac{1}{4\pi r_s^2} \iint_{\Omega_{r_s}} u_{rel} d\sigma \tag{4}$$

$$u_{slip} = u_{slip} e \tag{5}$$

where Re number $|u_{slip}| = u_{slip} = u_{in}$; $Re_p = \rho d_p u_{in} / \mu$; Re_p is particle Reynolds number, u_{slip} is the slip velocity; u_{in} is fluidization wind speed or incoming flow speed; d_p is the true diameter of the particle.

2.3 Fluent-based simulation of abrasive cell flow field

Since abrasive cell finishing is a relatively innovative processing method in the whole field of finishing, the simulation of gas–solid two-phase flow in the field of finishing is basically in a blank period, so this experiment refers to the simulation of fluidized bed in gas–solid two-phase flow and the analysis of molecular dynamics to simulate the internal flow field of the abrasive cell.

A simplified model of the abrasive cell processing cell and the volume of abrasive particles in the cell is shown in Fig. 3. The upper end of the model is the pressure outlet, the lower part is the airflow inlet, and the airflow speed is set to 0.5 m/s. The black part is abrasive, and the volume accounts for 20% of the overall volume of the abrasive cell. The solid phase of the simulation setup is the abrasive used in the processing of the abrasive cell, and the gas phase of the simulation is air at standard atmospheric pressure and room temperature of 20 °C. It is assumed that the solid phase is a rigid sphere and the gas phase is an ideal gas, and the parameters of the two phases are set as shown in Table 1.

The simulation of this experiment uses a two-fluid model, and the model defaults to 2D. It is known from the two-phase parameters that there is no chemical reaction between the gas phase and the solid phase during the fluidization process, which means that the physical parameters of the two phases do not change when it is fluidized, so time is chosen to be steady (steady-state). The remaining set parameters are shown in Table 2.

Figure 4 shows the volume diffusion diagram of abrasive under the action of gas, and Fig. 4a shows the flow pattern of abrasive grains of 24-mesh large particles. It can be seen

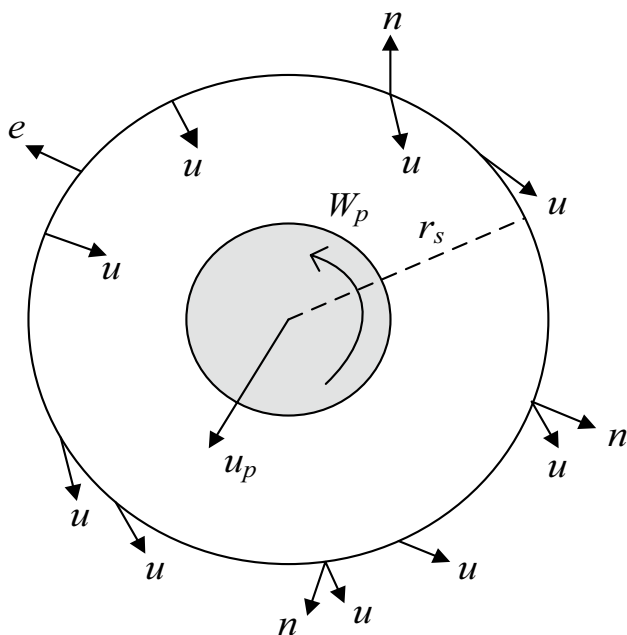


Fig. 2 Schematic diagram of slip velocity calculation



Fig. 3 Simplified model of abrasive pool

Table 1 Two-phase parameters

Parameter	Numerical value	Unit
Solid phase	Aluminum oxide	
Mean diameter	0.7/0.18/0.12	mm
Particle density	3950	kg/m ³
Bulk density	1990	kg/m ³
Gas phase	Nitrogen (standard atmospheric pressure, 20 °C)	
Density	1.225	kg/m ³
Viscosity	1.789×10^{-5}	Pa·s

from the figure that the 24-mesh abrasive grains are affected by the gas flow, and the bed of abrasive rises to, under the action of continuous wind, the middle abrasive grains, forming a flow state similar to the bubble flow, while the abrasive grains at the wall are not yet able to form a stable fluidized state due to the Saffman force and the traction force of the gas on the abrasive grains. Figure 4 b shows the adjusted volume distribution of abrasive grains and the flow pattern of 24-mesh large abrasive grains after adjusting the gas flow rate to 0.4 m/s. It can be found that the volume of abrasive grains rises more highly, and comparing Fig. 4a with Fig. 4b, it can be seen that the flow pattern of gas–solid two-phase flow reaches more stable volume and the abrasive grains are dispersed relatively more uniformly. Figure 4 c shows the flow pattern of abrasive grain volume after adjusting the abrasive grain to 80 mesh, and it can be seen that the volume of abrasive in Fig. 4c is more uniformly distributed and there is no abrasive vacuum area; compared with the above two cases, the flow pattern formation is more stable, which is beneficial to the processing of abrasive grain. From the comparison of Fig. 4 b and c, it can be seen that as the abrasive particle size decreases, the sliding speed of abrasive particles becomes larger, and the more dense area of gas vector distribution also moves from the exit and wall to the middle area, and the particles are subjected to more uniform force near the middle area, which is more favorable for polishing the workpiece.

From the simulation results, the gas–solid two-phase flow can fluidize the abrasives and transform them from a single stacked state to multiple fluid states. The subsequent experiments can set the air compressor speed to 0.2–0.4 m/s, which corresponds to the bulk flow state, turbulent flow state, and spraying flow state, respectively. The abrasive particle velocity reaches the maximum when it is close to the wall, so after adding the workpiece, the side of the workpiece may become the location with the highest processing efficiency, and choosing the appropriate abrasive flow state can make the workpiece increase the processing area and improve the processing efficiency. So from the theoretical point of view, gas–solid two-phase flow in the light finishing process is feasible.

3 Abrasive pool polishing experiment and analysis

3.1 Comparative experiment of abrasive pool machining and barrel grinding

3.1.1 Experimental condition

The workpieces selected for processing in this experiment are three common shapes, round pipe, square pipe, and

cylinder. Plate selection widely used Q235 steel plate material, and the mechanical properties and composition of the workpieces are tabulated in Table 3.

According to the three-dimensional motion law of the abrasive particles in the abrasive pool and different processing conditions, the abrasive particles are selected as sintered alumina abrasive. The meshes of the particle sizes were 60, 80, and 120. Sintered alumina is suitable for grinding or polishing high-carbon steel, high-speed steel, and hardened steel, with high hardness and high temperature resistance.

The abrasive pool finishing experiment was carried out on a three-axis milling machine, and the processing time was 5 min as a cycle. The schematic diagram of the experimental device is shown in Fig. 5. The abrasive pool is fixed on the working table of the machine tool through a fixed device to ensure that the various parts of the abrasive pool work normally, and the workpiece is driven by the spindle of the machine tool to achieve the workpiece at different speeds.

After finishing the workpiece by micro-cutting with high-speed abrasive flow, the surface morphology of the workpiece is detected to verify the finishing performance.

3.1.2 Experimental measuring instrument

Figure 6 a shows the machined workpiece that was measured using a Mitutoyo roughness measuring instrument for the five marked points in turn, and Fig. 6b shows the finished workpiece that was scanned using a Hitachi SU8010 electron microscope. The effect of the abrasive cell on the workpiece finishing process was evaluated by measuring the surface roughness of the workpiece together with observing the microscopic morphology of the workpiece.

3.1.3 Experimental procedure

The control variable method was used for the experiment. Experiment A was an abrasive tank processing experiment under the action of gas–solid two-phase flow. The outlet pressure of the air compressor was adjusted to make the abrasive form a stable loose flow state. Experiment B is an ordinary roller grinding experiment; the air compressor does not work, and the other experimental conditions are the same. The circular tube was selected as the workpiece to be processed, the abrasive particles were selected as 80 mesh,

Table 2 Setting of the two-fluid model

Parameter	Acceleration of gravity (g)	Outlet pressure (P)	Inlet gas velocity (V)	Pool height (H)	Pool width (L)	Number of time steps (T)	Maximum iteration number (T_{max})	Time step (T_{cfd})
Numerical value	9.8 m/t ²	0 MPa	0.5 m/s	420 mm	240 mm	2000	20	0.01 s

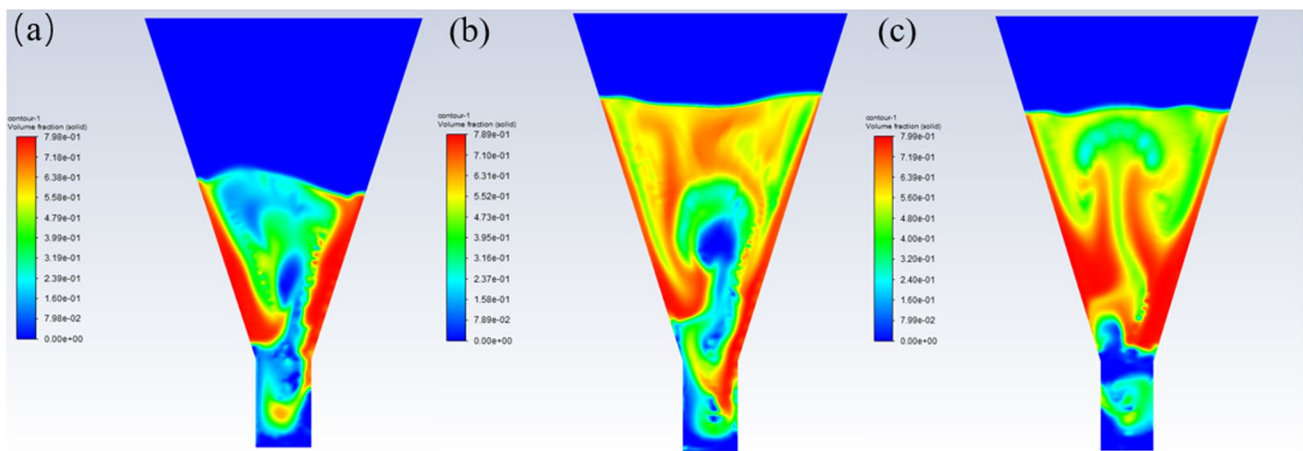


Fig. 4 a–c Abrasive particle diffusion diagram

Table 3 Workpiece parameter

Material	Yield strength (MPa)	Hardness (HB)	Melting point (°C)	C (%)	Mn (%)	Si (%)	S (%)
Q235	235	165	1600	0.12–0.20	0.3–0.65	0.3	0.05

Fig. 5 Schematic diagram of processing test bench

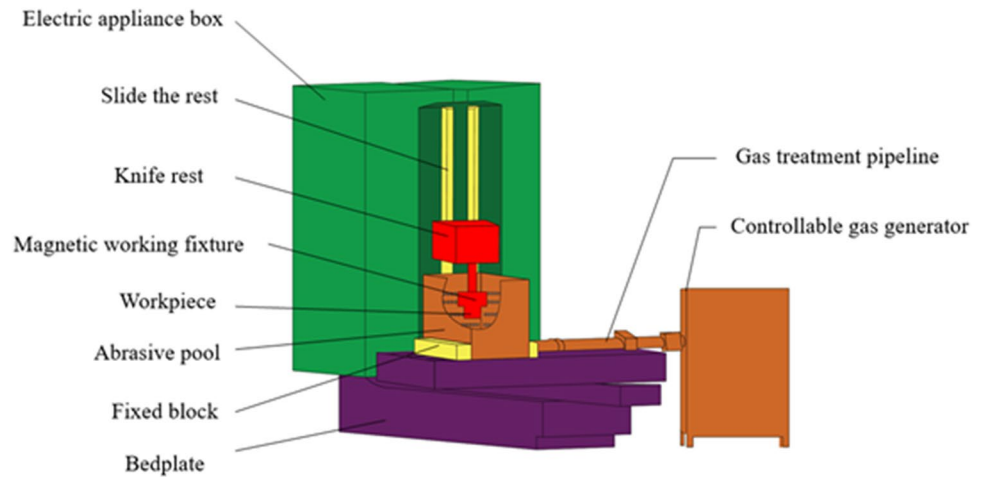
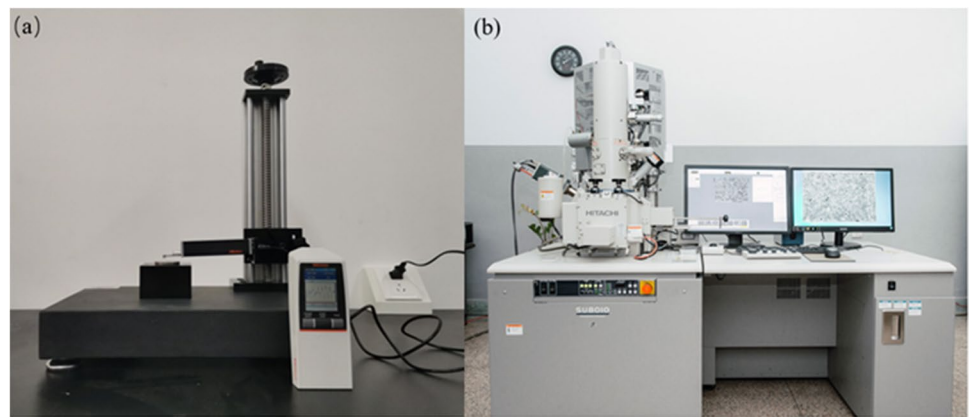


Fig. 6 Measuring instrument chart. **a** Japan Mitutoyo roughness measuring instrument. **b** Hitachi scanning electron microscope SU8010



and the wind speed of the air compressor was set as 0.4 m/s. When the abrasive particles formed a steady gas–solid two-phase flow under the action of the wind, the spindle speed was set as 750 rpm and the processing time was 5 min each time. The polishing was stopped after five times of processing, and the experimental data were recorded. After data recording, the second control experiment was carried out, and the procedure was the same as above under the condition of 120-mesh abrasive.

Abrasive particles will be fluidized during gas–solid two-phase flow processing, which theoretically results in a larger processing area as well as processing efficiency compared to normal tumbling processing. From a hydrodynamic point of view, the flow rate is most uniform when the abrasive is in the center of the workpiece. When the abrasive flows to the boundary, the abrasive flow rate increases, resulting in uncontrolled abrasive flow rate and weakened polishing effect, which may lead to uneven processing. Therefore, parameter acquisition for different locations can better detect the uniformity of abrasive pool processing. As Fig. 7 shows a round tube workpiece, the surface quality is observed to determine whether the abrasive cell processing has advantages in the finishing process on the curved surface, and five



Fig. 7 Workpiece physical drawing

inspection points are set to detect the surface processing quality of the workpiece.

3.1.4 Experimental results and analysis

As can be seen from Fig. 8, the turning point of the rough polishing stage from the sharp processing state to the smooth processing state is slightly delayed, and the surface roughness of the abrasive pool finishing process is slightly lower than that of the roller polishing process, thus indicating that with the gradual reduction of the abrasive mesh, the effect of the gas–solid two-phase flow on the surface of the workpiece was more obvious, and the processing characteristics of the

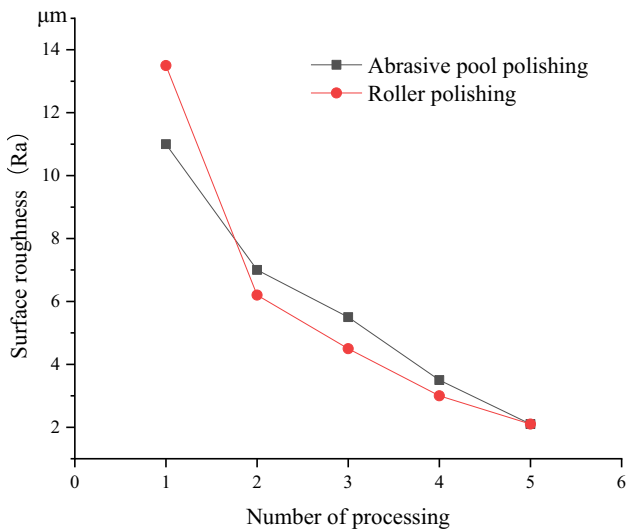


Fig. 8 Roughness comparison between roller grinding process and abrasive pool process in rough polishing stage

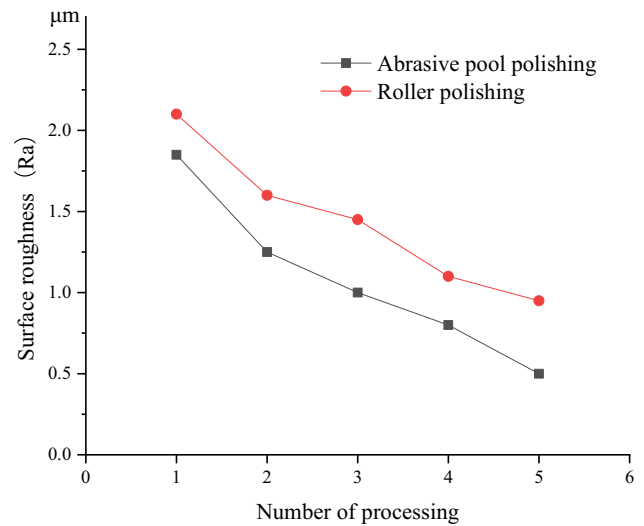


Fig. 9 Roughness comparison between roller grinding process and abrasive pool process in fine polishing stage

abrasive pool processing also gradually change to fluid. The smaller the abrasive, the lower the pressure exerted by the air compressor to ensure a stable flow pattern, and the lower the shear stress on the workpiece by the abrasive according to fluid mechanics, the more uniform the abrasive cell processing will be. The final result of the abrasive cell process may be better than that of the roller polishing process.

Figure 9 shows the surface roughness comparison of the fine polishing experimental workpiece. The final surface roughness Ra value of the roller grinding finishing process is 0.8 μm , while the surface roughness Ra value of the abrasive pool processing can reach 0.5 μm . After consulting the data, we found that the polishing curve of its abrasive pool processing is similar to the liquid float finishing process, which indicates that the gas–solid two-phase flow can play a greater role in the polishing of the workpiece.

Figure 10 shows the physical picture of the workpiece after processing, Fig. 10a is the abrasive cell processing, and Fig. 10b is the roller polishing processing. Figure 11 shows the SEM electron microscope picture of both, Fig. 11a is the electron microscope picture of Fig. 10a, and Fig. 11b is the electron microscope picture of Fig. 10b. From the picture, we can see that the surface scratches of the abrasive cell processing are less, the surface after processing is smooth, and almost there are no pits. The surface of the workpiece after roller grinding processing is darkened and has a small amount of pits. Through analysis, the reason for the dark surface is that when the workpiece is processed, the spindle speed is fast and the cutting force between the abrasive and the workpiece is too large, which causes the surface temperature of the workpiece to rise rapidly and cannot dissipate heat in time, and the surface of the workpiece becomes

carbonized and black after processing. When the abrasive pool is processed, the abrasive grains are in fluidization, the cutting force between the abrasive grains and the workpiece is smaller, and the air compressor has been continuously delivering air, so the heat can be dissipated in time when processing, so the surface of the workpiece has less scratches and the surface has a metallic luster after processing.

Figure 12 shows the comparison of roughness of points 1, 2, and 3 in two stages of roller grinding processing and abrasive pool processing; Fig. 12b shows the comparison of roughness of points 1, 2, and 3 after rough polishing; and Fig. 12c shows the comparison of roughness of points 1, 2, and 3 after semi-finishing polishing. It can be found that the surface roughness Ra value of point C processed with roller polishing is the lowest at 1.69 μm during rough polishing, but there is still a gradient difference in the surface roughness of the three points. The surface roughness using abrasive pool processing further reduces the gap compared with that when descaling, the extreme difference is only 0.15 μm , and the surface roughness is basically the same as that after roller grinding processing. After the fine polishing experiment, it can be more clearly observed that the surface uniformity of the workpiece processed by the abrasive pool is much better than that of the roller grinding process, and the surface roughness is also lower than that of the roller grinding process.

Through the experiment, it can be seen that the effect of abrasive cell processing is better than that of roller grinding processing. In order to further understand the advantages of abrasive cell finishing processing, orthogonal experiments were conducted to determine the best combination of parameters for abrasive pool processing.

Fig. 10 Comparison of work-piece drawings. **a** Abrasive pool processing. **b** Roll grinding process

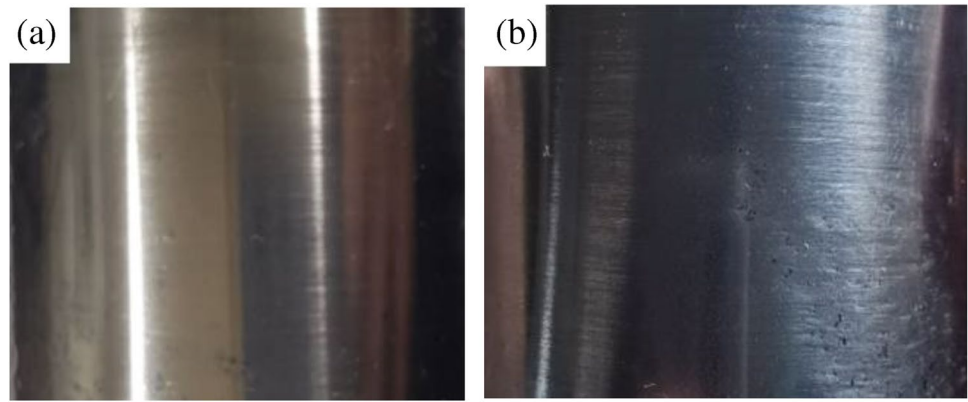


Fig. 11 SEM electron microscope contrast. **a** Abrasive pool processing SEM diagram. **b** Roller grinding process SEM diagram

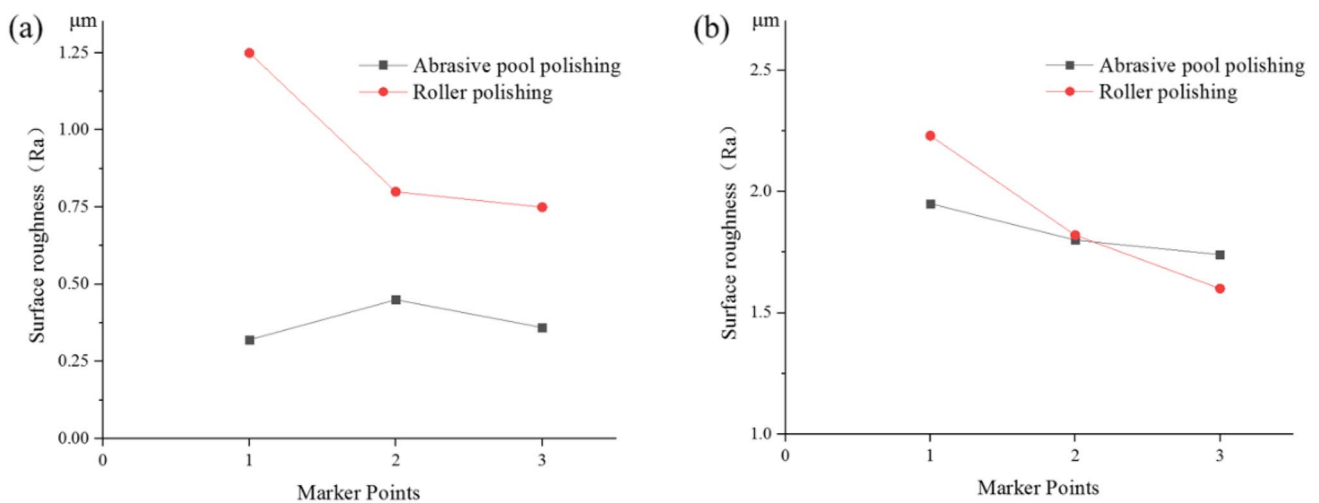
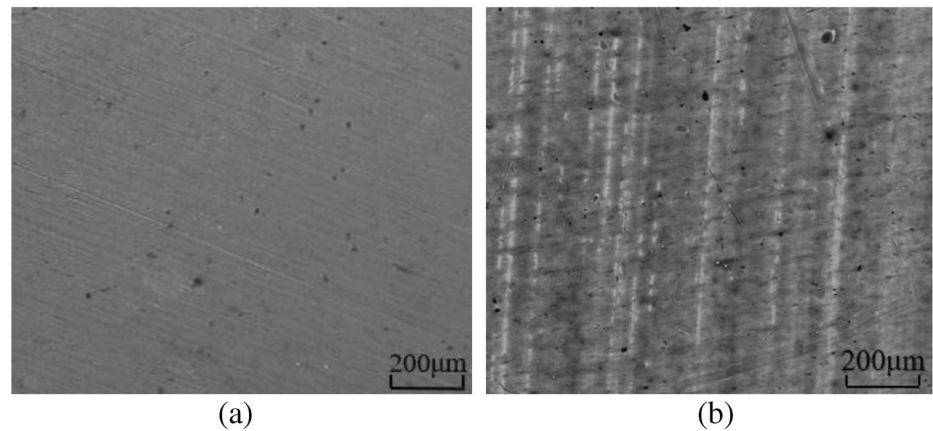


Fig. 12 Comparison of roughness of marking points between roller grinding and abrasive pool machining. **a** Surface roughness of marking points after rough polishing. **b** Surface roughness of marking points after precision polishing

3.2 Abrasive pool processing parameters on surface quality

3.2.1 Orthogonal experimental design

In this paper, the orthogonal experiment decides to choose the workpiece shape, abrasive size, gas–solid two-phase flow pattern, abrasive shape, and spindle speed as the key factors. The parameter setting range is listed in Table 4.

As there are many factors involved, the number of experiments can be reduced as much as possible without reducing the experimental effect. In this paper, the experimental method of orthogonal experiment is adopted. Using orthogonal experiment can quickly obtain the optimal solution of the experiment; because of the large difference in the level of each factor, it is necessary to choose the orthogonal experiment method at different levels.

According to Table 1, the standard orthogonal experimental table of $L_9(4^3)$ with four factors and three levels can be obtained after the particle shapes are completed by the quasi-horizontal method. The orthogonal experimental table is shown in Table 5.

As the gas–solid two-phase flow pattern, workpiece shape, and abrasive particle shape are all dimensionless factors, the above three parameters are digitized for the convenience of orthogonal experiment. The gas–solid two-phase flow pattern can be replaced by the Reynolds number, and the value range is set to 2000, 4000, and 6000. Workpiece shape can be replaced by the workpiece and abrasive flow contact surface. The contact between the pipe workpieces and the abrasive flow is generally the whole surface, the square pipe contact is four planes, and the cylindrical contact is the bottom plane. The three values are digitized and replaced by 1/3, 4/3, and 1/2, respectively. There are two types of abrasive shapes, spherical and irregular, which can be represented by the numbers 1 and 2. In order to test the overall effect of abrasive pool processing, it is necessary to ensure the continuity of the experiment, so the same workpiece is divided into three stages for experimental testing, that is, the workpiece is in the orthogonal experiment of 24-, 80-, and 120-mesh abrasive, respectively, during which the experimental workpiece will not be replaced, but the experimental measurement is still needed for each stage of processing. According to the experimental results, the spindle speed, workpiece shape, abrasive grain shape, gas–solid two-phase flow state, and other factors are analyzed to determine the influence of different machining parameters on the surface quality.

After the experiment, the roughness instrument was used to measure the surface roughness of the workpiece, and five detection points were set up to detect the surface machining quality of the workpiece.

Table 5 Orthogonal experiment table

Experiment	Spindle speed (rpm)	Gas–solid two-phase flow pattern	Work-piece shape	Abrasive particle shape
1	600	2000	1/3	1
2	600	4000	4/3	2
3	600	6000	1/2	2
4	900	2000	4/3	2
5	900	4000	1/2	1
6	900	6000	1/3	2
7	1200	2000	1/2	2
8	1200	4000	1/3	2
9	1200	6000	4/3	1

3.2.2 Experimental results and analysis

First, the surface roughness of each marked point of the pipework under 24-mesh abrasive was analyzed by intuitive analysis method. Table 6 shows the roughness value of the mark point of the pipe under orthogonal experimental conditions.

In order to fully analyze the polishing effect of the workpiece, it is necessary to analyze the results of each point. An example is given through the analysis of point 1. The following table shows the mean and range of surface roughness changes at point 1. K in the table represents the sum of surface roughness changes measured by different factors at the same level. K_1-K_3 is the rust removal experiment, K_4-K_6 is the rough polishing experiment, and K_7-K_9 is the fine polishing experiment. K represents the average value of different factors at the same level. R stands for range, $R = K_{max} - K_{min}$. The greater the range, the greater the influence of this factor on finishing processing. A, B, C, and D are used to replace the spindle speed, gas–solid two-phase flow pattern, workpiece shape, and abrasive particle shape in the processing factors, respectively, and the lower corner markers 1, 2, and 3 are the corresponding level 1, level 2, and level 3 of this factor, respectively.

It can be seen from Table 7 that the range of factor D is the smallest during abrasive pool processing, indicating that the abrasive particle shape has the least influence on the surface roughness. The maximum range of C indicates that

Table 4 Orthogonal experiment parameter range setting

	Processing parameters			
	Shape of the workpiece	Gas–solid two-phase flow pattern	Shape of abrasive grains	Spindle speed (rpm)
Level 1	Circular duct	Dispersion fluidization state	Sphere	600
Level 2	Square tube	Turbulent fluidization state	Irregular	900
Level 3	Cylindrical	Spurting fluidization state	–	1200

Table 6 The roughness height of circular tube marking point by orthogonal experiment

Mark point	Surface roughness Ra (μm)				
	1	2	3	4	5
Experiment number					
Mesh number of particle sizes 24					
1	4.722	4.815	4.778	4.746	4.784
2	5.521	5.539	5.515	4.572	4.608
3	5.123	5.215	5.146	5.214	5.159
4	5.349	5.368	5.336	4.875	4.881
5	5.002	5.108	5.023	5.114	4.947
6	4.933	4.875	4.903	4.891	4.835
7	4.965	4.932	4.895	5.037	4.992
8	4.633	4.571	4.584	4.619	4.592
9	5.381	5.414	5.392	4.988	5.049
Mesh number of particle sizes 80					
10	1.5370	1.505	1.5169	1.4811	1.4918
11	1.8562	1.9713	1.8965	1.6513	1.7079
12	1.6822	1.6345	1.5911	1.6847	1.6260
13	1.8215	1.9043	1.8854	1.5732	1.5137
14	1.5831	1.6426	1.5732	1.6469	1.5893
15	1.5850	1.6266	1.5924	1.6045	1.6100
16	1.6792	1.7340	1.6880	1.7128	1.6651
17	1.5098	1.5106	1.4947	1.5195	1.4955
18	2.3048	2.1338	2.2140	1.6521	1.5822
Mesh number of particle sizes 120					
19	0.4861	0.4893	0.5127	0.4921	0.5048
20	0.8921	0.9551	1.0361	0.6918	0.7244
21	0.6864	0.7340	0.6914	0.7186	0.6896
22	1.1817	1.2291	1.2006	0.8968	0.9724
23	0.4905	0.5201	0.3897	0.4943	0.5121
24	0.6282	0.5998	0.6039	0.5877	0.5825
25	0.5335	0.5564	0.5464	0.5687	0.5489
26	0.3903	0.4034	0.3943	0.4073	0.4156
27	1.4082	1.5913	1.4959	1.1192	1.2086

the workpiece shape has the greatest influence on the surface roughness of the workpiece. As the spindle drives the workpiece to rotate during the process, the different shapes of the workpiece will directly affect the stability of the abrasive in the abrasive pool, which in turn affects the polishing effect. With the decrease of abrasive and the improvement of polishing quality, it can be seen that the influence of gas–solid two-phase flow state on the workpiece gradually increases, and the range value gradually increases from 0.401 to 0.9397 μm at the beginning. With the improvement of machining quality, the proportion of abrasive particle shape to workpiece gradually increases. Through range analysis, it can be seen that the optimal combination to obtain the lowest roughness has always been $A_3B_2C_1D_2$, namely the spindle speed is 1200 rpm, gas–solid two-phase flow state for

turbulent flow, the shape of round tube, grinding grain shape is irregular shape, illustrates the essence of until the final experiment, the biggest effect on the machining performance is still the workpiece shape.

However, only through the average value and the range, it is impossible to judge the quantitative judgment of which factors have the greatest impact on the surface processing effect of the workpiece at which level, need to do with the result of orthogonal factors trend diagram, continue to point 1 as an example, according to the average roughness to assess, under the same factor, which way is the minimum surface roughness. This indicates that the level is the optimal level. The abscissa represents the different levels of different factors, while the ordinate represents the surface roughness value during processing, and finally forms the trend chart of factors, as shown in the figure.

As can be seen from Fig. 13, the trend of factor C in the same experimental stage changes greatly, indicating that the workpiece shape has the greatest influence on the abrasive pool processing. With the increasing precision of the experimental machining, the number of abrasive particles decreases, and the influence of gas–solid two-phase flow pattern on the machining effect becomes more and more obvious, from relatively flat at the beginning to fluctuating at the later stage, indicating that the influence of gas–solid two-phase flow pattern and abrasive shape on the roughness of the machined workpiece is gradually increasing. The slope of factor B_1 – B_3 increases gradually, indicating that the abrasive grains of 120 mesh may still be relatively large for abrasive pool processing and not the most suitable for abrasive pool processing. It can be speculated that the most suitable abrasive pool processing may be more precise finishing processing.

As can be seen from the figure above, the optimal combination of derusting experiment at point 1 is $A_3B_1C_1D_2$, the optimal combination of rough polishing experiment is $A_2B_2C_1D_3$, and the optimal combination of fine polishing experiment is $A_1B_2C_1D_2$.

By analogy, the three stage experiments of the remaining test points were comprehensively analyzed to obtain the influence degree of each factor and the optimal parameter combination table of all the points. The more times the factors and levels appear in the optimal combination, the more influence they have on the surface machining quality of the workpiece. According to the results of all stages, the influence degree of each factor on workpiece is as follows: workpiece shape, abrasive flow state, motor speed, and abrasive shape.

3.2.3 Analysis of workpiece surface topography

Figure 14 shows the SEM images and surface contour curves of three kinds of workpieces after finishing polishing, and

Table 7 Range analysis results of point 1

	Spindle speed (A)	Gas–solid two-phase flow pattern (B)	Shape of the workpiece (C)	Shape of abrasive grains (D)
K_1	15.336	15.036	14.288	15.105
K_2	15.248	15.156	16.251	15.419
K_3	14.979	15.437	15.09	15.105
K_4	5.0754	5.0377	4.6318	5.4249
K_5	4.9896	4.9491	5.9825	5.1204
K_6	5.4938	5.572	4.9445	5.0135
K_7	2.0646	2.2013	1.4946	2.3848
K_8	2.2904	1.7729	3.482	2.0438
K_9	2.332	2.7128	1.7104	2.2584
k_1	5.122	5.012	4.763	5.035
k_2	5.095	5.052	5.417	5.140
k_3	4.933	5.146	5.03	5.035
k_4	1.6918	1.6792	1.5439	1.8083
k_5	1.6632	1.6497	1.9941	1.7068
k_6	1.8312	1.8573	1.6481	1.6711
k_7	0.6882	0.7337	0.4982	0.7949
k_8	0.7634	0.5909	1.1606	0.6812
k_9	0.7773	0.9042	0.5701	0.7528
R_1	0.387	0.401	1.963	0.314
R_2	0.4184	0.6229	1.3507	0.3045
R_3	0.2672	0.9397	1.9872	0.3408
Maximum influencing factors in rust removal stage	C	B	A	D
Maximum influencing factors in rough stage	C	B	A	D
Maximum influencing factor in the fine throwing stage	C	B	D	A

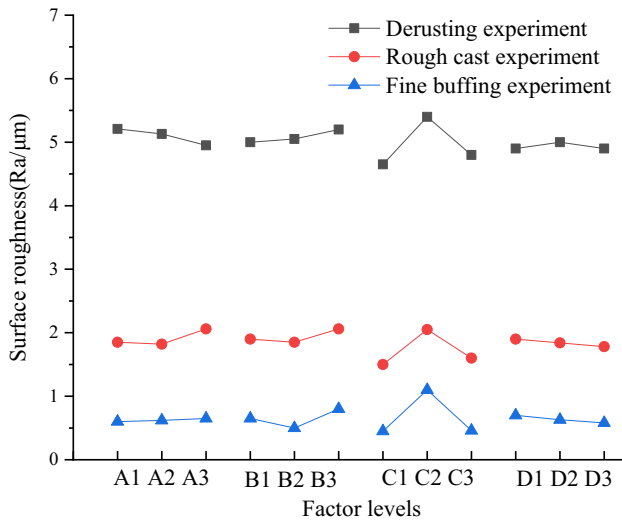


Fig. 13 Factor trend of point 1 by test

Fig. 15 shows the samples of three kinds of workpieces after wire-cutting.

Figure 14 a shows the SEM image of the cylindrical workpiece before machining; it can be seen that the surface rust of the unmachined workpiece is obvious, the surface profile is corrugated, and the surface roughness Ra is 42 μm. Figure 14 b shows the resulting graph of orthogonal experiment No. 20, where the motor spindle speed is 600 rpm, the machining abrasive particles are irregularly shaped, and the machined workpiece is a square tube. The surface roughness Ra is 0.734 μm. Figure 14 c shows the results of the orthogonal experiment No. 26, where the spindle speed is 1200 rpm, the abrasive grain is spherical, and the machined workpiece is a round tube. The surface roughness Ra is 0.403 μm. Figure 14 d shows the results of the orthogonal experiment No. 25 with a spindle speed of 1200 rpm, irregularly shaped abrasive grains, and a cylindrical workpiece. After descaling, the original milling grain of the workpiece will be exposed, but due to the low cutting force provided by the loose flow state formed by the abrasive, the machining efficiency is lower in the same machining time, resulting in the machining grain removal on the surface of the workpiece

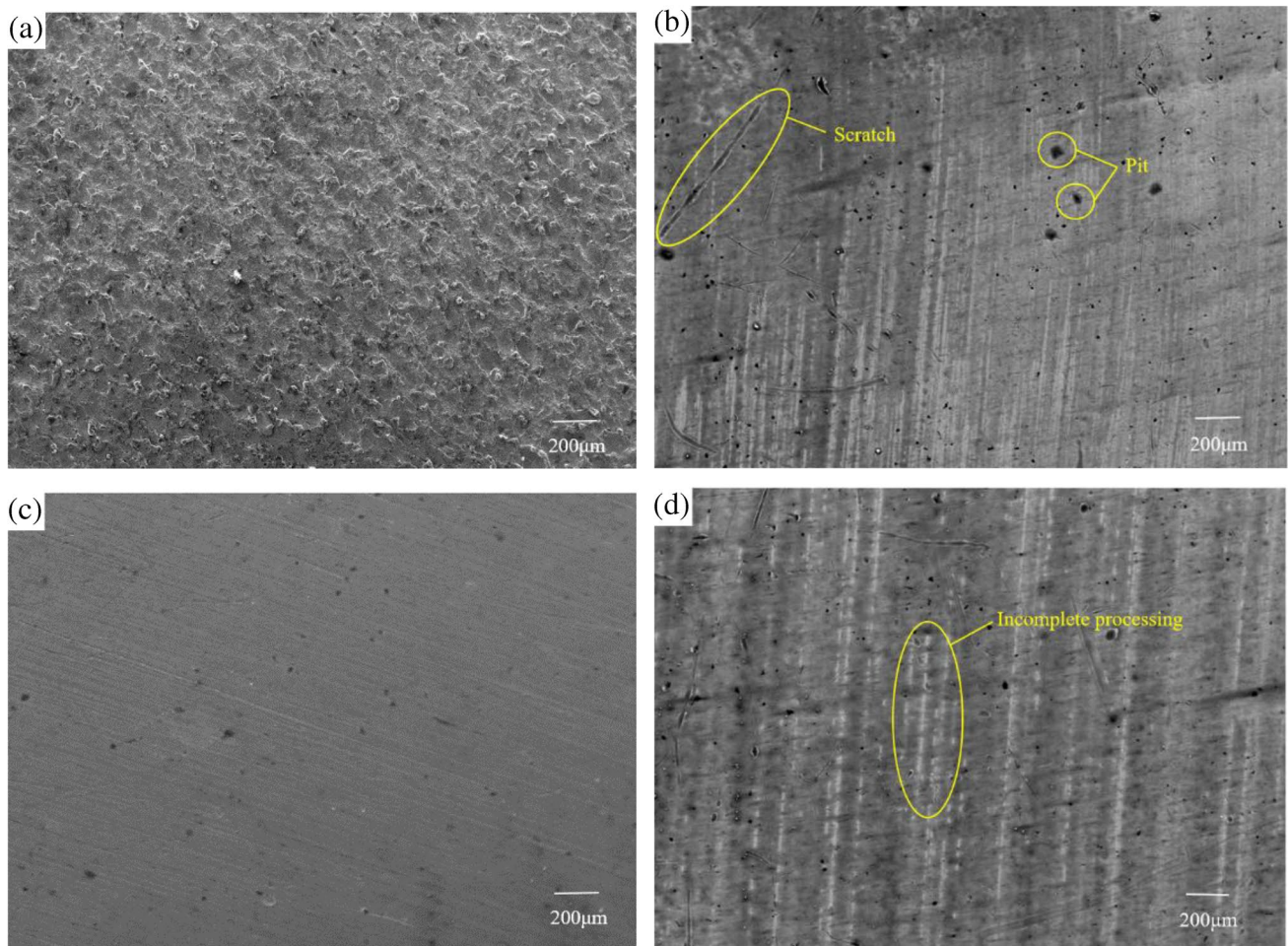
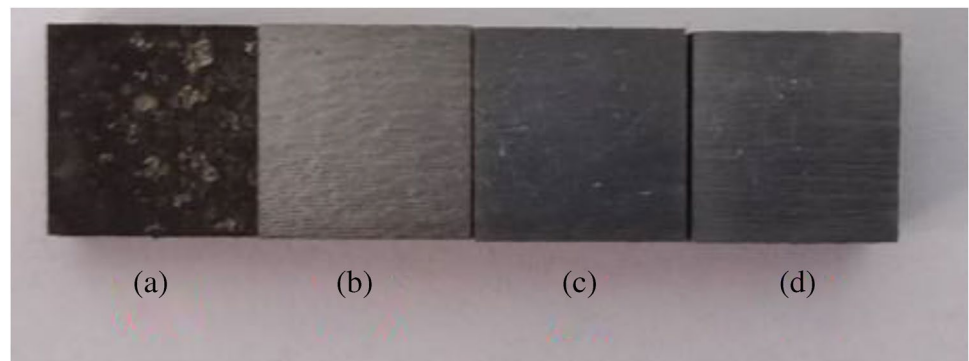


Fig. 14 Surface profile and microscopic topography of workpiece after fine polishing

Fig. 15 Observation sample

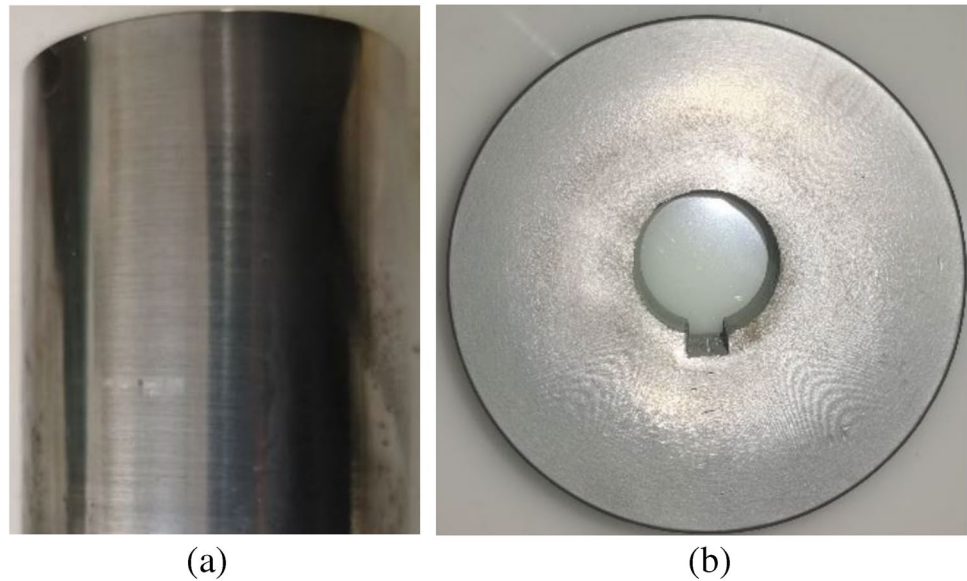


at the final finishing polishing that is not complete, and the root of the grain still remains on the surface of the workpiece. The scattered flow pattern is denser, with fewer bubbles between the abrasives, so the surface scratches and pits, and other defects are fewer after machining, and the surface roughness R_a is $0.628 \mu\text{m}$. Figure 16 shows the physical picture of the round tube and cylindrical workpiece after

finishing, and it can be seen that after polishing, the surface of the round tube is smooth and shiny, while the bottom surface of the cylinder has obvious milling pattern; it can be confirmed at the same time that abrasive pool finishing process on the side polishing effect is higher.

In conclusion, the turbulent flow state has the best processing effect in the same time, which is consistent with the

Fig. 16 Workpiece of the fine polish. **a** Tubular workpieces. **b** Cylindrical workpiece



results of the orthogonal experiment. However, if the time cost is not considered and the polishing experiment is carried out on the workpiece, the machining effect of abrasive in the dispersive flow state is better than that in the turbulent flow state. By comparing the initial workpiece with the finished workpiece, it can be seen that the surface quality of the workpiece has been greatly improved.

4 Conclusion

High-efficiency, high-precision, low-cost, pollution-free finishing is the goal of modern finishing field. Although there are more mature finishing methods at present, there are more or less certain limitations. Aiming at the above problems, a finishing method of pneumatic suspension abrasive pool was proposed, and the experimental platform was designed and built. Relevant research were carried out and the following conclusions were drawn:

1. Based on the micro-cutting principle of abrasive suspension motion, the gas–solid two-phase flow machining mechanism of abrasive particles in the abrasive pool was analyzed, the mixing and diffusion law of gas and abrasive in the abrasive pool was revealed, and the feasibility of pneumatic suspension abrasive pool finishing processing method was verified.
2. Select the key factors affecting the processing of the abrasive pool and design the orthogonal test, the experimental study on the characteristics of the polishing abrasive pool processing, the experimental results are very poor analysis of influence factors on the workpiece surface roughness is obtained the primary and secondary

relations of workpiece shape (circular tube) and flow state in gas–solid two-phase flow (turbulent flow), spindle speed (1200 rpm), grinding grain shape (the ball). The processing effect of abrasive pool was observed. Under the optimal experimental parameters, the processing lines on the surface of the workpiece were completely removed without holes and carbonation, and the surface of the workpiece was smooth, which could effectively improve the processing efficiency and quality of the workpiece surface. A new method is provided for machining complex curved parts in aerospace and other fields in the future.

Author contribution Investigation, data curation, formal analysis, visualization, software, writing—original draft, and writing—review and editing: Q.G. Formal analysis and software: W.W., X.L. Conceptualization, methodology, resources, supervision, and writing—review and editing: B.C. Supervision and review—editing: X.W. All authors have read and agreed to the published version of the manuscript.

Funding This work has been partly supported by Key R&D project of Shandong Province (2019GGX104081, 2019GGX104033), National Natural Science Foundation of China (No. 51805299), Shandong Province’s Key Support Regions Introducing Urgently Needed Talent Projects, and Young Innovative Talents Introduction and Training Program Project of Shandong Provincial Department of Education.

Data availability The raw/processed data required to reproduce these findings cannot be shared at this time, as the data also form part of an ongoing study that cannot be shared at this time, due to technical or time limitations.

Declarations

Conflict of interest The authors declare no competing interests.

References

- Alam Z, Jha S (2017) Modeling of surface roughness in ball end magnetorheological finishing (BEMRF) process. *Wear* 374:54–62. <https://doi.org/10.1016/j.wear.2016.11.039>
- Grover V, Singh A (2018) Modelling of surface roughness in a new magnetorheological honing process for internal finishing of cylindrical workpieces. *Int J Mech Sci* 144:679–695. <https://doi.org/10.1016/j.ijmecsci.2018.05.058>
- Mandal S, Thomas E, Gines L, Morgan D, Green J, Brousseau E, Williams O (2018) Redox agent enhanced chemical mechanical polishing of thin film diamond. *Carbon* 130:25–30. <https://doi.org/10.1016/j.carbon.2017.12.077>
- Lin Z, Wang R, Jhang Z (2018) Establishing a theoretical model for abrasive removal depth of silicon wafer chemical mechanical polishing by integrating a polishing times analytical model and specific down force energy theory. *The International Journal of Advanced Manufacturing Technology* 95(9):4671–4683. <https://doi.org/10.1007/s00170-016-9345-2>
- Guo L, Wang Z, Zhong S, Bao Q, Guo Z (2018) Fluidization state monitoring using electric current during fluidized bed reduction of iron ore. *Powder Technol* 343:683–692. <https://doi.org/10.1016/j.powtec.2018.11.058>
- Wang L, Qi G, Li Z, Zhang S, Hassan M, Liu X, Lu H (2019) Numerical simulation of flow behavior of topped gas-particles jet in a bubbling fluidized bed. *Powder Technol* 348:51–64. <https://doi.org/10.1016/j.powtec.2019.02.032>
- Pietrobono F, Rubino G, Tagliaferri V, Trovalusci F (2019) Sample position inside abrasive fluidized bed to obtain morphology uniformity. *The International Journal of Advanced Manufacturing Technology* 103(1):49–61. <https://doi.org/10.1007/s00170-019-03539-y>
- Chen K, Bachmann P, Bück A, Jacob M, Tsotsas E (2019) CFD simulation of particle residence time distribution in industrial scale horizontal fluidized bed. *Powder Technol* 345:129–139. <https://doi.org/10.1016/j.powtec.2018.12.086>
- Grigorov P, Muzzio F, Glasser B (2019) Modeling fluidized bed impregnation of active pharmaceutical ingredients onto porous excipients. *Chem Eng Sci* 202:36–54. <https://doi.org/10.1016/j.ces.2019.02.029>
- Uzi A, Levy A (2018) Energy absorption by the particle and the surface during impact. *Wear* 404:92–110. <https://doi.org/10.1016/j.wear.2018.03.007>
- Zheng C, Liu Y, Chen C, Qin J, Zhang S (2017) Finite element analysis on the dynamic erosion process using multiple-particle impact model. *Powder Technol* 315:163–170. <https://doi.org/10.1016/j.powtec.2017.04.016>
- Jiang Y, Fan X, Li T, Xiao S (2018) Influence of particle-size segregation on the impact of dry granular flow. *Powder Technol* 340:39–51. <https://doi.org/10.1016/j.powtec.2018.09.014>
- Shahin S, Reza S, Borhan M, Saeed Z (2021) The impact of SiC, Al₂O₃, and B₂O₃ abrasive particles and temperature on wear characteristics of 18Ni (300) maraging steel in abrasive flow machining (AFM). *Int J Hydrogen Energ* 46(68):33991–34001. <https://doi.org/10.1016/j.ijhydene.2021.04.051>
- Pathak C, Dodkar P (2020) Effect of shot blasting and shot peening parameters on residual stresses induced in connecting rod. *Trans Indian Inst Met* 73(2):571–576. <https://doi.org/10.1007/s12666-020-01866-3>
- Kaijalainen A, Vili K, Jouko H, Raimo R, Porter D, Kömi J (2018) Bendability of shot blasted ultrahigh-strength steels. *Mater Sci Forum* 941:510–515. <https://doi.org/10.4028/www.scientific.net/MSF.941.510>
- Zhang T, Wang S, Abdullahi Y, Jiang Z, Fang J, Fu X, Men X (2021) Study on the dynamic fatigue performance of shot blasting machine's blades based on modal analysis. *J Phys Conf Ser* 1948(1). <https://doi.org/10.1088/1742-6596/1948/1/012214>
- Wu J, Liu H, Wei P, Zhu C, Lin Q (2020) Effect of shot peening coverage on hardness, residual stress and surface morphology of carburized rollers. *Surf Coat Tech* 384(C):125273–125273. <https://doi.org/10.1016/j.surfcoat.2019.125273>
- Chen Y, Wang J, Gao Y, Feng A (2019) Effect of shot peening on fatigue performance of Ti 2 AlNb intermetallic alloy. *Int J Fatigue* 127:53–57. <https://doi.org/10.1016/j.ijfatigue.2019.05.034>
- Kovacı H, Bozkurt Y, Yetim A, Aslan M, Çelik A (2019) The effect of surface plastic deformation produced by shot peening on corrosion behavior of a low-alloy steel. *Surf Coat Tech* 360:78–86. <https://doi.org/10.1016/j.surfcoat.2019.01.003>
- Liu H, Jiang C, Chen M, Wang L, Ji V (2019) Surface layer microstructures and wear properties modifications of Mg-8Gd-3Y alloy treated by shot peening. *Mater Charac* 158(C):109952–109952. <https://doi.org/10.1016/j.matchar.2019.109952>
- Silva K, Carneiro J, Coelho R, Pinto H, Brito P (2019) Influence of shot peening on residual stresses and tribological behavior of cast and austempered ductile iron. *Wear* 440(C): 203099–203099. <https://doi.org/10.1016/j.wear.2019.203099>
- Maleki E, Unal O, Kashyzadeh K (2019) Surface layer nanocrystallization of carbon steels subjected to severe shot peening: analysis and optimization. *Mater Charac* 157(C): 109877–109877. <https://doi.org/10.1016/j.matchar.2019.109877>
- Pritima D, Dhinakaran V, Stalin B, Ravichandran M, Balasubramanian M, Anand Chairman C (2020) Surface roughness prediction and parametric optimization of shot blasting of Al7068 using RSM. *IOP Conference Series: Materials Science and Engineering* 988(1):012100. <https://doi.org/10.1088/1757-899X/988/1/012100>
- Mohamed A, Zoheir F, Andrew W, James G (2018) Effect of a Moving Automated Shot Peening and Peening Parameters on Surface Integrity of Low Carbon Steel. *J Mater Process Tech* 277. <https://doi.org/10.1016/j.jmatprotec.2019.116399>
- Lim L, Lim E (2019) Mixing and segregation behaviors of a binary mixture in a pulsating fluidized bed. *Powder Technol* 345:311–328. <https://doi.org/10.1016/j.powtec.2019.01.026>
- Namdardedenji R, Hashemnia K, Emdad H (2018) Effect of flow pulsation on fluidization degree of gas-solid fluidized beds by using coupled CFD-DEM. *Adv Powder Technol* 29(12):3527–3541. <https://doi.org/10.1016/j.apt.2018.09.033>
- Lv B, Luo Z, Zhang B, Qin X (2018) Particle motion and separation behavior of coal in gas–solid separation fluidized bed. *Powder Technol* 339:344–353. <https://doi.org/10.1016/j.powtec.2018.08.013>

Publisher's Note Springer Nature remains neutral with regard to jurisdictional claims in published maps and institutional affiliations.

Springer Nature or its licensor (e.g. a society or other partner) holds exclusive rights to this article under a publishing agreement with the author(s) or other rightsholder(s); author self-archiving of the accepted manuscript version of this article is solely governed by the terms of such publishing agreement and applicable law.